INT. J. REMOTE SENSING, 2002, VOL. 23, NO. 11, 2247–2262

Taylor & Francis
Taylor & Francis Group

View angle effects on canopy reflectance and spectral mixture analysis of coniferous forests using AVIRIS

D. B. LOBELL, G. P. ASNER*,

Department of Global Ecology, Carnegie Institution of Washington, Stanford, California 94305, USA

B. E. LAW

Oregon State University, College of Forestry, Oregon State University, Corvalis, Oregon 97331, USA

and R. N. TREUHAFT

Jet Propulsion Laboratory, California Institute of Technology, Pasadena, California 91109, USA

(*Received 4 April 2000; in final form 16 March 2001*)

Abstract. The dependence of vegetation reflectance on sun and sensor geometry can potentially provide information on canopy properties, but also may be a source of unmodelled systematic error in single-angle remote sensing measurements. In this study, we investigated the angular variability of reflectance measurements from the NASA Airborne Visible/Infrared Imaging Spectrometer (AVIRIS), and the resulting impact on spectral mixture analysis (SMA) using both full-range (400–2500 nm) and shortwave-infrared wavelengths (2080–2280 nm; *AutoSWIR*). The study was conducted in coniferous forests in Central Oregon using five AVIRIS overpasses to generate multiple view angle measurements. Canopy reflectance was highly anisotropic, with the strength of the angular signal controlled by species type, canopy cover and soil reflectance. Canopy cover estimates from full-range SMA averaged only slight decreases (~6% relative) toward the retro-solar direction for 16 field plots in the study region. *AutoSWIR* was even less influenced by view angle, exhibiting changes only for large differences in view angle. In addition, *AutoSWIR*'s ability to accommodate endmember variability led to stronger agreement with field cover values than full-range SMA. The results suggest that while view angle can significantly affect reflectance measurements from AVIRIS, the consequent variability in vegetation cover estimates from SMA and *AutoSWIR* is low.

1. Introduction

The influence of solar and viewing geometry on the observed reflectance of a surface is described by its bidirectional reflectance distribution function (BRDF). In the case of vegetation canopies, the BRDF can be highly anisotropic due to three-dimensional canopy and landscape structure (e.g. Li and Strahler 1985, Goel 1988,

* e-mail: greg@globalecology.stanford.edu

International Journal of Remote Sensing
ISSN 0143-1161 print/ISSN 1366-5901 online © 2002 Taylor & Francis Ltd
http://www.tandf.co.uk/journals
DOI: 10.1080/01431160110075613

Myneni *et al*. 1989), leaf optical properties (Walter-Shea and Norman 1991) and soil reflectance (Jacquemoud *et al*. 1992). In the traditional context of nadir remote sensing, the BRDF was viewed as a source of error for reflectance measurements from wide swath sensors, such as the National Oceanic and Atmospheric Administration (NOAA) Advanced Very High Resolution Radiometer (AVHRR) (Meyer *et al*. 1995). Numerous studies, however, have demonstrated that measurements from multiple-view angles can provide unique information on atmospheric and surface properties (e.g. Asner *et al*. 1998, Diner *et al*. 1999). For example, multi-angle measurements often reveal structural differences between species that appear similar from single-angle measurements (e.g. Kleman 1987, Sandmeier and Deering 1999).

While the information content of multi-angle data is now recognized, the angular dependence of BRDF is still ignored in many studies, and presents a potential source of systematic error. In particular, the NASA Airborne Visible and Infrared Imaging Spectrometer (AVIRIS) is used to study land surface and atmospheric properties with high spectral resolution observations (Green *et al*. 1998). However, with an angular field-of-view of 30°, AVIRIS encounters view zenith angles of up to 15° to each side of nadir, which can result in significant BRDF effects in the imagery (e.g. Kennedy *et al*. 1997). While most BRDF studies have focused on sensors designed to acquire data from a wide range of angles, relatively few have addressed the impact of angular variations in BRDF on measurements from AVIRIS (e.g. Kennedy *et al*. 1997, Mustard *et al*. 2001).

In addition, although many studies have investigated the view-angle dependence of vegetation metrics like the normalized difference vegetation index (NDVI; Privette *et al*. 1995), the effect of viewing geometry on other remote sensing signatures and methods has not been adequately addressed. One of the most common applications in vegetation remote sensing is spectral mixture analysis (SMA), which is used to estimate the fractional cover of major scene components, or endmembers (e.g. green vegetation, soil and shade), in each image pixel (e.g. Roberts *et al*. 1993, Smith *et al*. 1994, Bateson and Curtiss 1996). The fractional extent of vegetation is important from biophysical and biogeochemical perspectives (Defries *et al*. 1999), as well as for investigating secondary sources of spectral variation (Asner 1998). Ideally, the inclusion of photometric (spectrally flat) shade as an endmember compensates for view angle effects by modelling the portion of each pixel that is blocked from direct sunlight. However, wavelength dependent multiple scattering in vegetation canopies results in shade that is not spectrally flat (e.g. Roberts *et al*. 1993). Therefore, there is some variability to be expected in SMA products due to viewing and solar geometry, although this effect has not, to our knowledge, been quantified.

Recent work toward more general SMA approaches with AVIRIS has resulted in a method termed *AutoSWIR* (Asner and Lobell 2000a,b). This approach employs only reflectance measurements in part of the shortwave–infrared region (SWIR2: 2080–2280 nm) to determine fractional covers of green vegetation, senescent vegetation (litter) and soil. Unlike traditional SMA, which typically uses the full range of visible, near-infrared (NIR), and SWIR wavelengths (~400–2500 nm), *AutoSWIR* does not include a shade endmember. Instead, the SWIR2 spectra are normalized by subtracting the reflectance at 2080 nm. The resulting 'tied' spectra are then unmixed using sets of field endmember spectra, which span a wide range of vegetation and soil types but possess low spectral variability in the space of tied SWIR2 spectra (Asner 1998, Asner and Lobell 2000a,b, Asner *et al*. 2000). The principal advantage

of *AutoSWIR* is that its generality allows cover estimates independent of the variability of soil and vegetation properties that hampers many full spectral range SMA efforts.

In this study, the AVIRIS instrument was repeatedly flown over temperate coniferous forests in Central Oregon on 10 June 1999, to acquire measurements of selected conifer forest targets from a range of view angles. A series of field plots in the region were simultaneously surveyed to characterize soil type, species distribution, canopy structure and other potential sources of variability in BRDF. The AVIRIS and field data were then used to (1) assess the view angle dependence of reflectance and (2) quantify the accuracy and angular variability of full spectral range SMA and *AutoSWIR* canopy cover estimates.

2. Methods

2.1. *Site description*

The study region of approximately 576 km^2 was located on the east side of the Cascade Mountains in Central Oregon, where there is a strong climatic gradient and forest transition from Douglas fir (*Pseudotsuga menziesii*) and grand fir (*Abies grandis*) in the west to the dry eastern extent of ponderosa pine (*Pinus ponderosa* var. Laws). Within this region, we located 20 100 m × 100 m plots along an east–west swathe that includes Douglas fir, grand fir, larch (*Larix occidentalis*), cedar and ponderosa pine forests (table 1). The sites encompassed a range of soil textures, stand densities (number of trees/area), canopy heights and other structural properties, as specified in table 1.

2.2. *Field measurements*

Within each 100 m × 100 m plot, we established five 10 m radius plots for measurements of canopy dimensions. Tree height and height to base of live crown of all trees > 5 cm diameter breast height (1.3 m) were measured using a laser system (Impulse 200 and Mapstar System, Laser Technology, Engelwood, CO, USA). Crown radius was measured with a tape from the centre of the main stem to the widest point of the crown. The remaining trees (< 5 cm dbh) were tallied. Soils data were acquired from the Soil Survey Geographic (SSURGO) database. Canopy cover estimates were derived using maximum likelihood classification of georeferenced low-altitude airphotos from 1997 (Lobell *et al.* 2001). The high spatial resolution of the airphotos (~2 m) allowed each pixel to be treated as a pure cover type, with ~2500 pixels falling within each plot.

2.3. *AVIRIS data*

The AVIRIS was flown over the study region on 10 June 1999 on the NASA ER-2 aircraft at 20 km altitude, creating approximately 17 m × 17 m pixels at nadir. Five consecutive overpasses were used to obtain multiple view angles, with flight paths and solar positions described in table 2. All paths were flown perpendicular to the solar principal plane in order to position the scan line of the sensor into and away from the Sun. Thus, we tried to position the scan lines in the Sun-view plane in which BRDF effects are most pronounced (Ranson *et al.* 1994, Russell *et al.* 1997, Gastellu-Etchegorry *et al.* 1999). Measured radiance values were converted to apparent surface reflectance using the Atmospheric Removal (ATREM) code (Gao *et al.* 1993), which employs the 6S scattering code for atmospheric gases (Vermote *et al.*

Table 1. Summary of vegetation structure and soil properties at field plots. Vegetation cover values were derived from low-altitude air-photo.

Plot	Altitude (m)	Species (trees per hectare)	Canopy height (m) Mean (Std)	Crown radius (m) Mean (Std)	Vegetation cover (%)	Soil texture	Soil class
1	911.7	Pipo (479)	11.5 (7.9)	4.9 (2.3)	62	Sandy loam	ALFIC VITRIXERANDS
2	905.4	Pipo (84)	33.5 (11.5)	4.0 (1.2)	49	Sandy loam	ALFIC VITRIXERANDS
3	912.5	Pipo (1276)	12.1 (6.9)	1.5 (1.0)	65	Sandy loam	ALFIC VITRIXERANDS
4	934.8	Pipo (299)	12.3 (14.0)	2.1 (1.4)	63	Sandy loam	ALFIC VITRIXERANDS
5	916.8	Pipo (388)	13.7 (5.9)	1.9 (0.7)	64	Sandy loam	ALFIC VITRIXERANDS
6	918	Pipo (866) Pipo (318)	11.8 (4.8)	1.5 (0.5)	68	Sandy loam	AQUIC VITRIXERANDS
7	914.7	Laoc (115) Abgr (76) Laoc (178)	17.6 (8.5)	1.7 (0.6)	73	Sandy loam	ALFIC VITRIXERANDS
8	911.5	Pipo (127) Abgr (25)	19.2 (10.8)	1.6 (0.7)	68	Sandy loam	ALFIC VITRIXERANDS
9	935.2	Pipo (210)	13.3 (3.9)	1.6 (0.4)	N/A	Very gravelly Loamy sand	UMBRIC VITRIXERANDS
10	1147	Pipo (255)	8.7 (2.4)	2.0 (0.5)	58	Sandy loam	ALFIC VITRIXERANDS
11	1250	Pipo (363) Abgr (407)	14.2 (2.9)	2.2 (0.5)	58	Sandy loam	XERIC VITRICRYANDS
12	986.9	Pipo (84) Cade (32) Laoc (8)	22.6 (N/A)	3.0 (0.7)	75	Very gravelly Loamy coarse sand	TYPIC VITRICRYANDS
13	936.4	Pipo (8) Abgr (4) Abgr (286)	28.4 (13.1)	2.7 (0.7)	N/A	Very gravelly Loamy sand	UMBRIC VITRIXERANDS
14	996.6	Psme (140) Pipo (57)	17.6 (4.6)	2.2 (1.1)	76	Very gravelly Loamy sand	UMBRIC VITRIXERANDS
15	924.1	Pipo (33)	23.5 (12.1)	2.8 (0.5)	55	Loamy sand	HUMIC VITRIXERANDS
16	922.1	Pipo (452) Pipo (318) Laoc (108)	15.2 (6.4)	1.8 (0.5)	83	Very gravelly Loamy sand	UMBRIC VITRIXERANDS
17	909.1	Pico (51) Psme (51) Cade (350)	12.7 (7.4)	1.4 (0.6)	73	Sandy loam	ALFIC VITRIXERANDS
18	1132	Pipo (115)	10.6 (9.7)	2.0 (1.4)	N/A	Sandy loam	ALFIC VITRIXERANDS
19	916.9	Pipo (306)	12.0 (4.8)	1.7 (0.6)	66	Sandy loam	ALFIC VITRIXERANDS
20	1185	Pipo (344)	4.3 (1.2)	1.2 (0.3)	N/A	Sandy loam	ULTIC HAPLOXERALFS

Species codes: Abgr = *Abies grandis*, Cade = *Calocedrus decurrens*, Lands = *Larix occidentalis*, Pico = *Pinus contorta*, Pipo = *Pinus ponderosa*, Psme = *Pseudotsuga menziessii*.
N/A = airphoto not available.

Table 2. Flight information for five AVIRIS overpasses on 10 June 1999 in Central Oregon.

AVIRIS path	Centre Lat. (°N)	Centre Long. (°W)	Heading (°E of N)	Time (Local)	Sun zenith angle (°)	Sun azimuth angle (°E of N)
1	44.51	121.76	65.43	11:14:40	23.92	149.81
2	44.47	121.77	65.20	11:26:58	22.91	156.26
3	44.43	121.79	65.32	11:39:07	22.13	163.12
4	44.39	121.78	65.45	11:51:22	21.60	170.42
5	44.35	121.80	65.39	10:57:00	25.64	140.67

1997). The images were georeferenced to within one pixel using tie-point matching with Geographical Information System (GIS) road coverages.

Bidirectional reflectance factors (BRFs) were calculated for each plot by extracting the average reflectance for a 3×3 pixel box surrounding the plot centres. View zenith angles were calculated from the plots' positions along the scan line, and were defined to be positive in the backscatter (northern) direction, and negative in the forward-scatter direction. Because of the extent of the study region and the spacing of the overpasses, each plot was viewed by at most three of the five overflights. The reflectance anisotropy was characterized at each wavelength with an anisotropy index (ANIX):

$$\text{ANIX} = \max\,(\text{BRF})/\min\,(\text{BRF}) \tag{1}$$

where the maximum and minimum BRF are taken over all flights (e.g. Sandmeier and Deering 1999). While solar zenith and azimuth angles changed slightly over the hour of image acquisition (table 2), and could therefore influence ANIX measurements, their effects were probably small compared to the relatively large changes in view zenith angles (e.g. Russell *et al.* 1997). None the less, it should be noted that ANIX is entirely an empirical measure and depends on the angles sampled for each site; therefore, only ANIX values from adjacent plots were analysed to assess sources of variation.

2.4. *Full-range spectral mixture analysis*

Full-range SMA ($\sim$400–2500 nm) was applied to reflectance data for all paths using four endmembers: green vegetation, litter, soil and photometric shade. The litter and soil endmembers were derived from the average of field spectra, acquired concurrently with image acquisition (Lobell *et al.* 2001; see figure 1). Field spectra of green canopies were not acquired owing to the height of the major species, but a vegetation endmember was derived from a region of dense vegetation in the image reflectance data. Fractions were computed for each pixel according to the SMA equations:

$$\rho_{\text{pixel}} = \sum \{\rho_{\text{e}}\, \text{C}_{\text{e}}\} + \varepsilon = \{\rho_{\text{veg}}\, \text{C}_{\text{veg}} + \rho_{\text{soil}}\, \text{C}_{\text{soil}} + \rho_{\text{litter}}\, \text{C}_{\text{litter}} + 0.0\, \text{C}_{\text{shade}}\} + \varepsilon \tag{2}$$

$$\sum \text{C}_{\text{e}} = 1.0 \tag{3}$$

where ρ and C are the reflectance and cover fraction of each endmember, respectively, and ε is an error term (the reflectance of shade is prescribed a constant value of 0.0). Equation (2) constrains the sum of fractions to equal 1.0, although individual fractions are not constrained between 0.0 and 1.0. Wavelengths with significant sensor noise or atmospheric water absorptions were omitted from the analysis, resulting in a total of 149 bands used for the SMA (460–910 nm, 965–1105 nm, 1535–1735 nm and 2070–2370 nm). The fraction of total green canopy cover was calculated as $\text{C}_{\text{veg}}(1-\text{C}_{\text{shade}})^{-1}$, in order to compensate for the shadowed portion of each pixel (e.g. Smith *et al.* 1990).

2.5. AutoSWIR

All AVIRIS scenes were also processed using the *AutoSWIR* algorithm, described in detail by Asner and Lobell (2000a,b). In short, tied SWIR2 spectra from the AVIRIS data were unmixed many ($n = 50$) times with the SMA equations (2) and (3), each time with a random combination of endmembers selected from field endmember databases. The resulting fractions from this Monte Carlo approach invariably possess

a normal distribution for each cover type, with a standard deviation indicative of the variability in the endmember spectra. Low variability within endmember classes is thus propagated to low uncertainty in the derived fractions. As mentioned, shade is not explicitly included as an endmember in *AutoSWIR*, but is inherently contained within the green canopy endmember variability (Asner 1998).

The endmember spectral databases used in *AutoSWIR* consisted of 17 litter and 30 soil spectra from field surveys in Oregon (Lobell *et al*. 2001), and 60 green canopy spectra from an extensive study of arid and semi-arid ecosystems (Asner 1998, Asner and Lobell 2000a,b). All spectra were resampled to AVIRIS wavelengths. Lobell *et al*. (2001) found that while using arid soils led to slight overestimates of green canopy fractions, the use of arid vegetation for lack of coniferous canopy spectra did not compromise *AutoSWIR* results. This is due to the generality of the SWIR2 reflectance shape of vegetation, which results from strong foliar water absorption. Figure 1(*a*)–(*c*) shows 10 representative full-range spectra for each endmember class, with the corresponding tied SWIR2 spectra in Figure 1(*d*)–(*f*). Note that while the image-derived vegetation endmember for full-range SMA (shown in bold) possesses much higher NIR reflectance than the arid vegetation spectra, its SWIR2 reflectance is well within the range of variability present in the endmember database.

2.6. *NDVI*

For comparison with the full-range SMA and *AutoSWIR* results, the NDVI was also calculated at each plot:

$$\mathrm{NDVI} = (\rho_{810\mathrm{nm}} - \rho_{680\mathrm{nm}})/(\rho_{810\mathrm{nm}} + \rho_{680\mathrm{nm}}) \tag{4}$$

Several studies have investigated the angular dependence of NDVI in coniferous forests, demonstrating a decrease in NDVI with increasing view angle (e.g. Ranson *et al*. 1994, Deering *et al*. 1994, 1999). This is due to greater multiple scattering of NIR photons than of visible photons, which causes the contrast between sunlit and shaded canopies to be more pronounced at visible wavelengths than in the NIR. (The NDVI decreases as visible reflectance increases more than NIR reflectance.)

Variability due to view angle for the full-range SMA, *AutoSWIR* and NDVI was quantified at each plot as the ratio of the endmember cover fraction (or NDVI value) retrieved in the backscatter direction (B) to that retrieved in the forward-scatter direction (F). The ratio B/F thus describes the magnitude and direction of change relative to F, with ratios less than one indicating a decrease in fraction (or NDVI value) in the backscatter direction. In addition, the accuracy of the SMA and *AutoSWIR* fractions were assessed by comparing retrieved fractions from the centre path (path 3 in table 2) to field cover estimates.

3. Results and discussion

3.1. *AVIRIS reflectance*

The reflectance of all plots increased with view zenith angle at all wavelengths, which is consistent with findings from other studies of coniferous forests (e.g. Johnson 1994, Bicheron *et al*. 1997, Russell *et al*. 1997). The consistent increase of reflectance with view angle also supports the notion that solar angle effects are small, since different plots were viewed at maximum view angle by different overflights. Figure 2 shows part of the study region as viewed from two different AVIRIS overpasses, demonstrating the significant brightness differences due to viewing geometry. Figure 3 shows the BRF for plot 1 from three different viewing angles, along with the

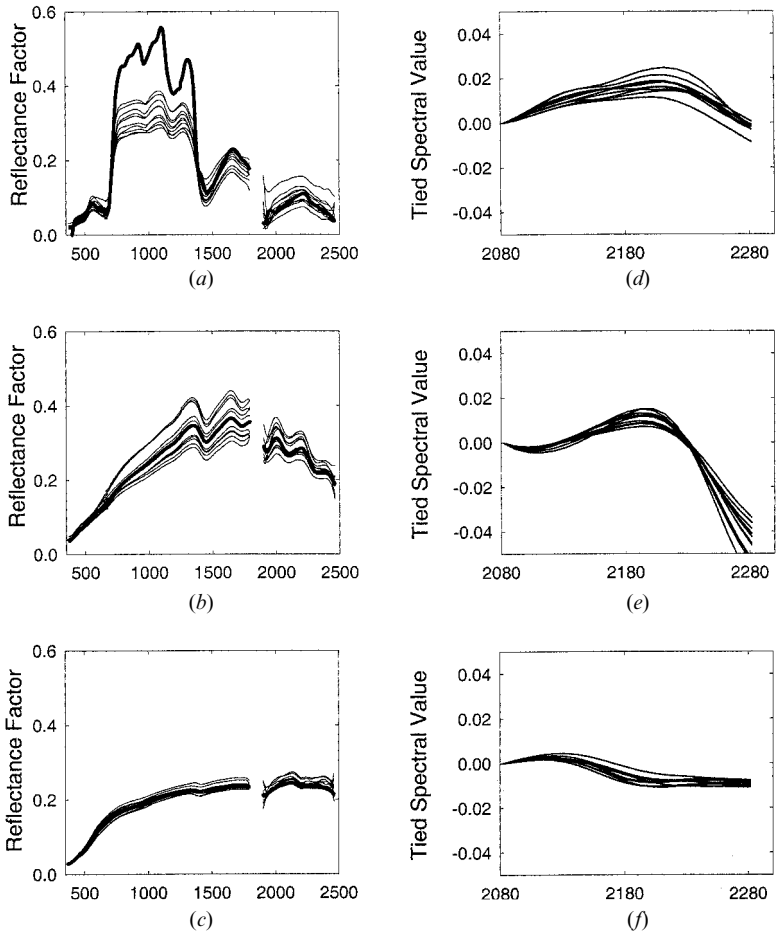

Figure 1. Representative spectra from (*a*) green canopy, (*b*) litter and (*c*) soil field spectral databases, demonstrating range of albedo variation. Endmembers used for full-range SMA are shown in bold. Tied SWIR2 endmembers used in AutoSWIR are shown in (*d*) to (*f*). X-axes are wavelengths expressed in nanometers.

calculated ANIX at each wavelength. With a solar zenith angle near 22°, the AVIRIS view angles did not encounter the sharp hotspot that results from complete canopy self-shadowing in the retro-solar viewing direction (Hapke *et al.* 1996). However, a significant increase in reflectance (87% at 680 nm in plot 1) from the forward-scatter to backscatter direction was still observed. No increase in reflectance was observed toward the forward-scatter direction for the range of angles sampled, although this effect has been seen for wider view angles (e.g. Deering *et al.* 1994). The ANIX spectra (Figure 3(*b*)) demonstrated that reflectance anisotropy reaches a maximum at visible wavelengths and a minimum in the NIR. As mentioned, the high reflectance and transmittance of NIR photons in the canopy leads to multiple scattering, which effectively decreases the contrast between shaded and sunlit canopies. The visible and SWIR wavelengths, in contrast, are strongly absorbed in the canopy and undergo minimal multiple scattering.

It is apparent in figure 3 that while visible reflectance is only slightly lower than

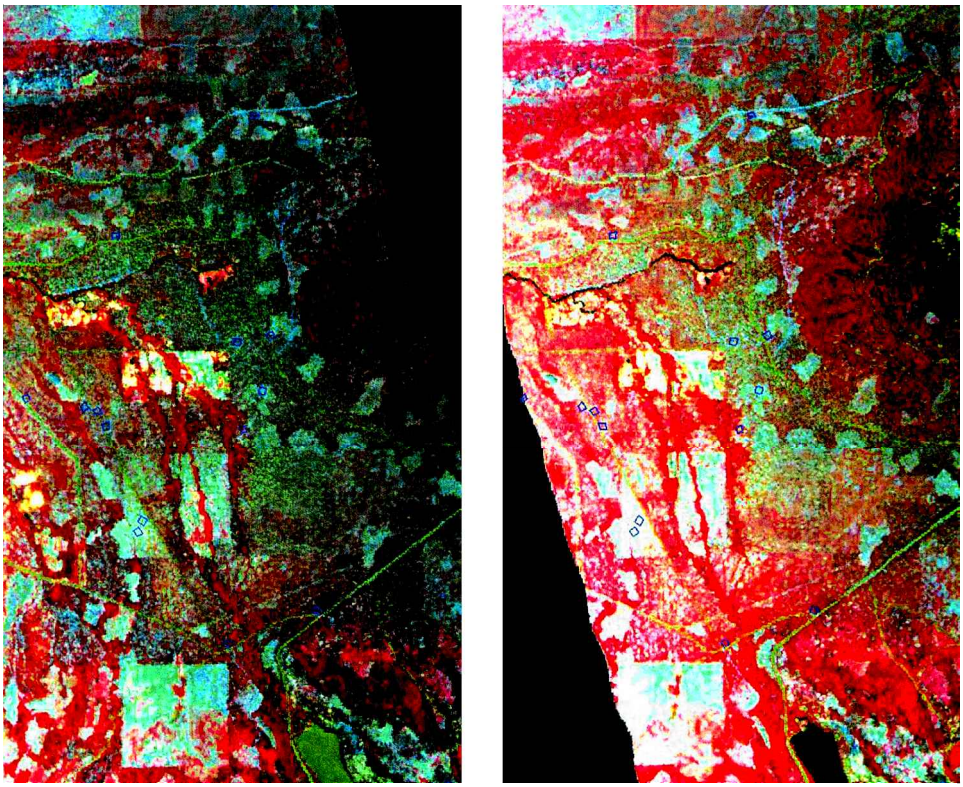

Figure 2. Colour composite reflectance image of study region as viewed from AVIRIS overpasses 3 (left) and 4 (right) (red: 810 nm, green: 680nm, blue: 2100 nm). Images are displayed with identical stretches, and field plots are outlined in blue. Reflectance is higher for backscatter viewing angle (path 4).

in the SWIR, its anisotropy is far greater. Thus, the absence of multiple scattering alone cannot explain the high reflectance anisotropy. Moreover, differences in down welling radiance between visible and SWIR cannot explain reflectance anisotropies, since ATREM corrects for the shape of the solar spectrum. In fact, we believe the large anisotropy observed for visible wavelengths is due in part to the strong anisotropic reflectance characteristics of aerosols in the atmosphere, which preferentially scatter in the retro-solar direction (e.g. Diner *et al.* 1999). ATREM does not correct for this angular effect because it assumes isotropic atmospheric scattering; therefore, it is important to consider the atmosphere when analysing apparent surface reflectance anisotropy in visible wavelengths (<700 nm). However, when addressing sources of variability in reflectance anisotropy for adjacent field plots (in the following paragraphs), we believe that variability in atmospheric properties plays a minor role.

No significant relationships were found between the observed reflectance anisotropy and mean canopy height, crown radius and/or soil properties. However, there was a discernible dependence of ANIX on the airphoto canopy cover estimates. Figure 4 shows the ANIX and canopy cover values for three different groups of plots. Each group represents plots that are within a small geographic range, in order to ensure that they were viewed by similar angles from each path. This avoids variability in ANIX due to viewing geometry, as discussed above. Each group shows

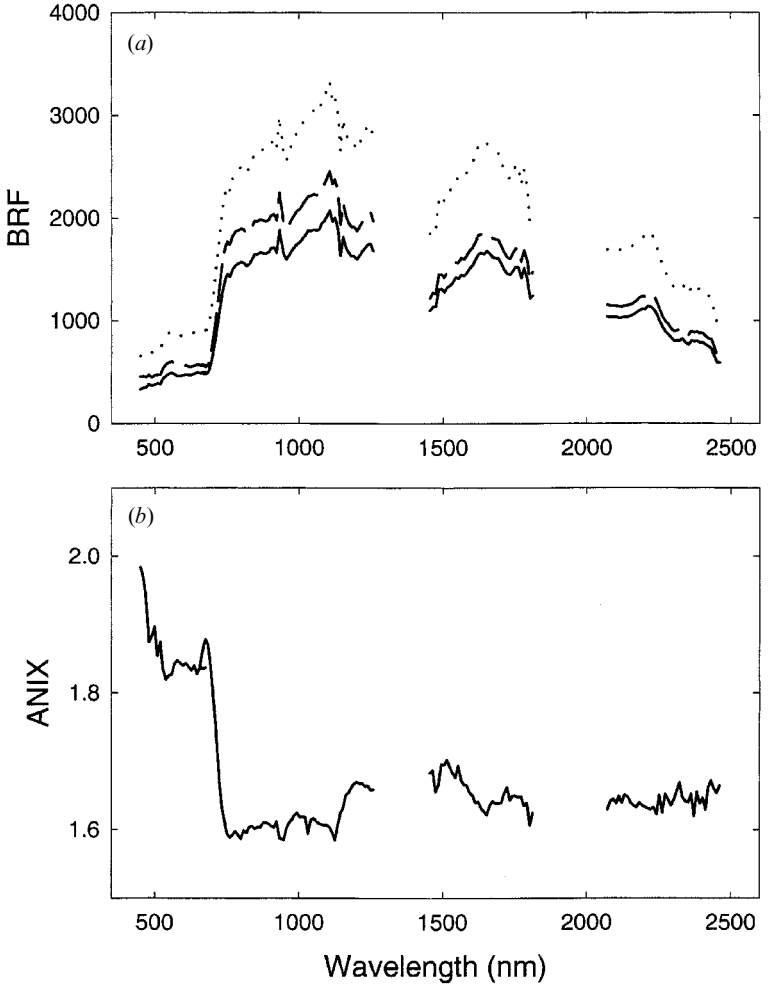

Figure 3. (*a*) Bidirectional reflectance factors (BRFs) and (*b*) ANIX spectra for plot 1 for three viewing angles: -10.62° (solid), 0.63° (dashed) and 11.55° (dotted).

a roughly linear increase in ANIX with canopy cover. This is similar to the findings of Johnson (1994), who found that reflectance anisotropy of pine forests was higher in denser stands due to the increased influence of shadows. However, the linear relation between angular reflectance and canopy cover appears to break down at cover below 60%, especially in the case of group 3 (figure 4). It is likely that at sufficiently low cover, soil reflectance becomes significant in the backscatter direction, but remains shaded for forward-scatter view angles. This contribution to backscatter reflectance causes the observed increase in reflectance anisotropy. In the other groups, plots are viewed from larger view angles and soil influences are therefore not as apparent.

Another noteworthy feature in figure 4 is the distinctly high ANIX value for one plot in the second group (plot 12), which was attributed to the dominance of *Abies grandis* and the large range of measurement angles. We speculate that the higher density of needles in *Abies grandis* (relative to ponderosa pine) creates more distinct

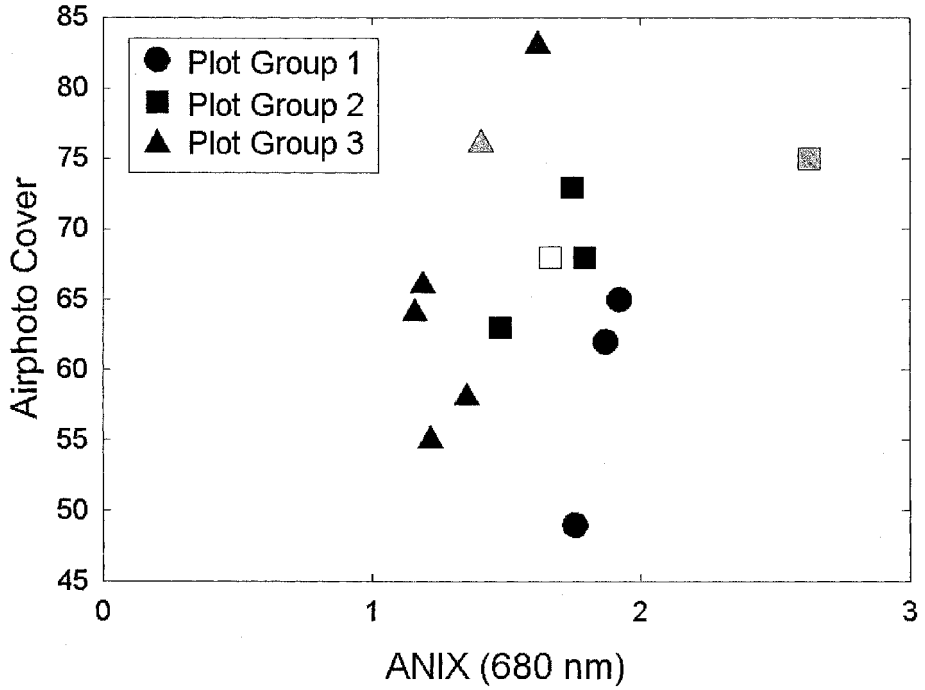

Figure 4. Canopy cover vs. ANIX at 680 nm for three plot groups. Shading indicates dominant species: *Pinus ponderosa* (black), *Abies grandis* (grey) and *Larix occidentalis* (white).

shadows that results in stronger anisotropic reflectance effects in the BRDF. While plot 14 was also dominantly *Abies grandis*, it did not exhibit strong reflectance anisotropy because it was not viewed at sufficiently large angles. These findings stress the interplay of view angle, species type, soil reflectance and canopy cover in determining the impact of BRDF. At larger view zenith angles ($>10^{\circ}$), species differences appear to dominate reflectance anisotropy, with canopy cover playing a secondary but important role. At smaller view angles, soil reflectance also becomes an important source of variability. Because large view angles were required to distinguish *Abies grandis* from *Pinus ponderosa*, only relatively small areas viewed from both extremes by AVIRIS could be mapped in this study for species differences. However, it is possible that species with distinct differences for smaller view angles could be separated with only a few AVIRIS overpasses. For larger view angle capabilities, such as with the Multi-angle Imaging Spectroradiometer (MISR; Diner *et al.* 1999), our findings would support the potential for species mapping with angular measurements (e.g. Sandmeier and Deering 1999).

3.2. *SMA,* AutoSWIR *and NDVI*

View angle effects on reflectance were modelled by SMA largely as a change in the shade fraction. This was manifested in a distinct gradient from relatively high shade in the south (up to 50%) to nearly shade-free pixels in the north (figure 5). However, the shade endmember failed to emulate perfectly the BRDF effect because of the spectral variability in reflectance anisotropy (figure 3), resulting in variability in the other endmembers as well. In particular, the canopy cover estimates from SMA changed by an average of $(-5.5 \pm 1.8)\%$ toward the hotspot direction

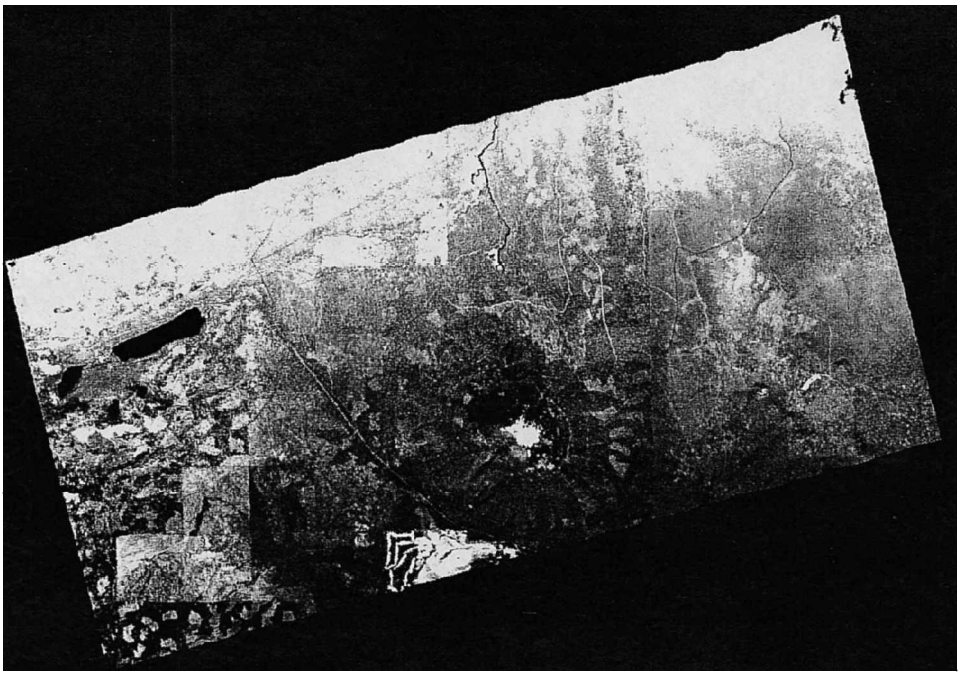

Figure 5. Shade fraction image for path 4, demonstrating decrease in canopy shade toward retro-solar direction. Display is linearly scaled from 0% shade (white) to 50% shade (black).

Table 3. Results for 16 field photos. B and F are values for backscatter and forward-scatter view angles, respectively. Cover fractions are given as percentages.

Plot	Airphoto cover	View zenith angle (°)		SMA cover		*AutoSWIR* cover		NDVI	
		Min (F)	Max (B)	Path 3	B/F	Path 3	B/F	Path 3	B/F
1	62	−10.6	11.6	56.6	0.95	60.6	0.94	0.46	0.89
2	49	−10.3	11.9	52.1	0.93	47.9	0.78	0.43	0.93
3	65	−10.8	11.3	67.9	0.90	70.0	0.94	0.55	0.90
4	63	−13.2	8.9	65.1	1.03	67.5	0.97	0.51	0.99
5	64	−6.1	5.3	62.6	1.03	62.1	1.03	0.51	1.02
6	68	−10.8	11.5	70.9	0.90	67.7	0.90	0.56	0.89
7	73	−10.6	11.6	62.8	0.93	72.5	0.95	0.55	0.91
8	68	−10.2	12.0	58.9	1.10	72.6	0.95	0.49	0.98
10	58	−11.7	10.1	62.5	0.95	58.7	0.98	0.53	0.95
11	58	−6.4	5.1	73.4	0.90	62.5	1.01	0.57	0.94
12	75	−13.2	9.2	92.0	0.82	69.7	1.05	0.68	0.86
14	76	−6.4	5.2	104.5	0.99	75.8	1.13	0.77	0.97
15	55	−6.6	4.9	35.6	0.95	56.4	0.95	0.38	0.96
16	83	−5.4	6.0	92.6	0.83	85.0	1.06	0.67	0.86
17	73	−8.0	3.2	73.8	0.92	75.9	0.90	0.57	0.91
19	66	−7.5	3.8	69.4	1.01	68.7	1.04	0.53	1.00

(mean $\pm$ standard error; table 3). Mean vegetation fractions from *AutoSWIR* demonstrated less of a decrease with view angle, with an average change of $(-2.7 \pm 2.1)\%$. The 16 plots used in the analysis were further divided into two classes: those viewed

by both larger ($\sim 10^\circ$) positive and negative view angles (plots 1–4, 6–10 and 12), and those with more modest view angle ranges ($\sim -5^\circ$ to 5°). Canopy cover estimates for the nine plots viewed from larger view angles varied by an average of $(-5.5 \pm 2.1)\%$ and $(-6.2 \pm 1.8)\%$ due to view angle for SMA and *AutoSWIR*, respectively. The second set of plots averaged $(-5.5 \pm 1.7)\%$ variability for SMA, and $(1.8 \pm 1.9)\%$ for *AutoSWIR*. Thus, SMA results were nearly identical for both sets of plots, while *AutoSWIR* results exhibited significant decreases only for the plots viewed from extreme angles. NDVI values changed by an average of $(-6.4 \pm 1.2)\%$, with an average of $(-7.8 \pm 1.1)\%$ and $(-4.6 \pm 1.3)\%$ change for the two plot classes, respectively.

The decrease in both NDVI and SMA cover estimates in the backscatter direction can be explained by the greater reflectance anisotropy for visible wavelengths than in the NIR. This results in a decreased contrast between red and NIR reflectance as shade becomes less prominent (e.g. Ranson *et al.* 1994, Deering *et al.* 1994, 1999). The average decrease in *AutoSWIR* green canopy fractions arises from the increase of SWIR2 reflectance in the backscatter direction (e.g. figure 3). This albedo increase magnifies the shape of the SWIR2 signature, leading to steeper SWIR2 tied spectra. For vegetation canopies, the increased reflectance contrast causes a sharper rise in reflectance from 2100–2200 nm, and a steeper decrease in reflectance from 2200–2300 nm (see figure 1). *AutoSWIR* modelled this effect largely as an increase in litter cover, which has a characteristic absorption from 2200–2300 nm, and a decrease in soil cover, which decreases in reflectance from 2100–2200 nm. In fact, while the average green vegetation cover for all plots decreased only from 71.4% for negative view angles to 69.5% for positive view angles, litter fractions rose from an average of 3.4% to 15.0% and soil fractions dropped from 25.2% to 15.4%. Thus, view angle had a much larger effect on litter and soil estimates than for vegetation fractions.

While the observed decreases in vegetation estimates were statistically significant for SMA (t-test, $p = 0.005$), B/F values were not significantly lower than 1.0 for *AutoSWIR* at the 90% confidence level ($p = 0.108$). Moreover, the distribution of B/F for the 16 plots was Gaussian (Kolmogorov test) with large standard deviations for both methods (7.4% for SMA; 8.3% for *AutoSWIR*). This suggests that even with a systematic decrease due to view angle, random processes, such as errors in reflectance calibration or co-registration, largely governed the differences in fractions from different view angles. We also note that changes in fractions are defined as a percentage of F; for example, an average decrease of -5% translates to only -2.5% for a region with 50% cover. Thus, we conclude that view angle introduces only a slight bias into vegetation cover estimates with AVIRIS, and may be unimportant relative to other sources of errors encountered in practical applications.

We have shown here only that variability due to viewing geometry is similarly small for SMA and *AutoSWIR* results. However, variability due to other factors, such as spectral variability of vegetation and soil surfaces, can be significantly different for the two approaches. Comparable variability with view angle thus does not necessarily translate to comparable overall performance. For example, figure 6 shows SMA and *AutoSWIR* results for the centre path in comparison to airphoto cover estimates. While SMA showed general agreement with field values, the correlation suffered from variability in vegetation and soil spectral properties across the scene.

The mean canopy fractions from *AutoSWIR*, which fundamentally accounts for natural variability (Asner 1998, Asner and Lobell 2000a,b), more accurately predicted

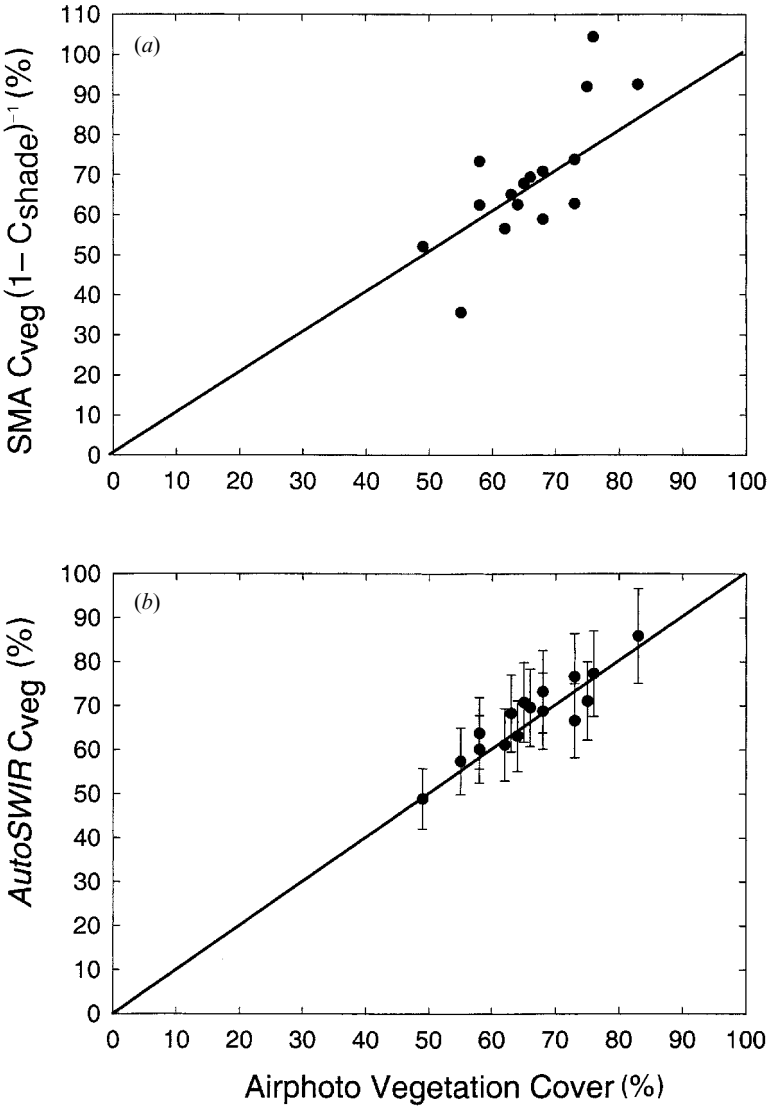

Figure 6. Canopy cover estimates (%) from (*a*) SMA and (*b*) *AutoSWIR* for path 3 compared to low-altitude airphoto estimates at field plots. Mean $\pm$ one standard deviation is shown for *AutoSWIR*'s Monte Carlo output.

vegetation cover at the plots. In addition, through its Monte Carlo approach, *AutoSWIR* provided an estimate not only of the mean (i.e. most likely) fraction, but also the likelihood of the true fraction being within a certain range. For example, figure 6(*b*) shows the mean fraction $\pm$ one standard deviation, or an approximate 67% confidence interval for the true fraction given all possible combinations of vegetation, litter and soil spectra in the field database. Interestingly, the mean fractions from *AutoSWIR* fell within one standard deviation of the field values for all plots. This was possibly due to an unusually lucky realization of the *AutoSWIR* procedure. However, more likely this was due to the fact that *AutoSWIR* assumes

that each database spectrum, representing a spectrum acquired in the field, can occur with equal probability. In reality, the extremely bright and dark spectra for each endmember are probably less likely to occur at the scale of the pixel than the more moderate spectra. *AutoSWIR*'s assumption of equal probability therefore overestimates the true variability in endmember spectra, resulting in conservatively wide confidence intervals. Although the algorithm could be modified to represent more accurately the distribution of endmember spectra, we feel that the current confidence intervals, while conservative, are satisfactorily small.

It is noteworthy that this study was specifically designed to embody the worst-case scenario for BRDF effects on AVIRIS reflectance and subsequent NDVI, full-range SMA and *AutoSWIR* products. In particular, it focused on coniferous forests that are notoriously anisotropic (Abuelgasim and Strahler 1994, Gastellu-Etchegorry *et al.* 1999), and the sensor was positioned in the solar principal plane where BRDF effects are most extreme (Myneni *et al.* 1997). Therefore, this study may provide an upper bound on the angular variability expected in canopy cover estimates from AVIRIS. However, further research with different vegetation species, soil types and solar angles would be needed to test this claim.

4. Conclusions

This study provided insight into BRDF effects in AVIRIS data and on canopy cover estimation techniques. Strong reflectance anisotropy of coniferous forests appeared to be primarily the result of canopy shading, which varied with species structural characteristics and overall canopy cover. Soil reflectance also contributed to the observed anisotropy, but only at sufficiently low cover. The dominance of species architecture in determining anisotropy supports the potential for species mapping with multi-angle data. However, other factors, such as canopy cover, can have important effects on reflectance anisotropy and should be considered in future studies.

Spectral mixture analysis using both full-range and SWIR wavelengths was largely successful in compensating for BRDF effects for the range of view angles in these AVIRIS data. This suggests that comparison of fractions from different viewing angles will introduce only a slight bias, provided that co-registration and spectral calibration is accurate. While full-range SMA was sensitive to changes in endmember spectra throughout the scene, *AutoSWIR* successfully accounted for both view angle and endmember variability. This demonstrates the potential of *AutoSWIR* for providing robust estimates of vegetation cover for land-use management, change detection and modelling research.

Acknowledgments

We thank K. Cody, S. Van Tuyl and S. Kerr for their field assistance and their contributions to data analysis. This study was supported by NASA OES grant NAG5-8320 (RTOP 622-93-63-40), and also by NASA New Investigator Program grant NAG5-8709 to G. Asner.

References

Abuelgasim, A. A., and Strahler, A. H., 1994, Modeling bidirectional radiance measurements collected by the Advanced Solid-state Array Spectroradiometer (ASAS) over Oregon transect conifer forests. *Remote Sensing of Environment*, **47**, 261–275.

Asner, G. P., 1998, Biophysical and biochemical sources of variability in canopy reflectance. *Remote Sensing of Environment*, **64**, 234–253.

Asner, G. P., and Lobell, D. B., 2000a, A biogeophysical approach for automated SWIR unmixing of soils and vegetation. *Remote Sensing of Environment*, **74**, 99–112.

Asner, G. P., and Lobell, D. B., 2000b, *AutoSWIR*: a general spectral unmixing algorithm based on 2000–2400 nm endmember datasets and Monte Carlo analysis. *Proceedings of the Airborne Science and Applications Workshop, NASA Jet Propulsion Laboratory, Pasadena, CA, USA, 21 January, 2000*, pp. 41–50.

Asner, G. P., Bateson, C. A., Privette, J. L., El Saleous, N., and Wessman, C. A., 1998, Estimating vegetation structural effects on carbon uptake using satellite data fusion and inverse modeling. *Journal of Geophysical Research*, **103**, 28 839–28 853.

Asner, G. P., Wessman, C. A., Bateson, C. A., and Privette, J. L., 2000, Impact of tissue, canopy and landscape factors on reflectance variability of arid ecosystems. *Remote Sensing of Environment*, **74**, 69–84.

Bateson, C. A., and Curtiss, B., 1996, A method for manual endmember selection and spectral unmixing. *Remote Sensing of Environment*, **55**, 229–243.

Bicheron, P., Leroy, M., Hautecouer, O., and Breon, F. M., 1997, Enhanced discrimination of boreal forest covers with directional reflectances from the airborne polarization and directionality of Earth reflectances (POLDER) instrument. *Journal of Geophysical Research*, **102**, 29 517–29 528.

Deering, D. W., Eck, T. F., and Middleton, E., 1994, Reflectance anisotropy for a spruce-hemlock forest canopy. *Remote Sensing of Environment*, **47**, 242–260.

Deering, D. W., Eck, T. F., and Banerjee, B., 1999, Characterization of the reflectance anisotropy of three boreal forest canopies in spring–summer. *Remote Sensing of Environment*, **67**, 205–229.

Defries, R. S., Field, C. B., Fung, I., Collatz, G. J., and Bounoua, L., 1999, Combining satellite data and biogeochemical models to estimate global effects of human-induced land cover change on carbon emissions and primary productivity. *Global Biogeochemical Cycles*, **13**, 803–815.

Diner, D. J., Asner, G. P., Davies, R., Muller, J.-P., Pinty, B., Schaaf, C. B., and Stroeve, J., 1999, New directions in Earth observing: scientific applications of multiple-view-angle remote sensing. *Bulletin of the American Meteorological Society*, **80**, 2209–2228.

Gao, B.-C., Heidebrecht, K. B., and Goetz, A. F. H., 1993, Derivation of scaled surface reflectance from AVIRIS data. *Remote Sensing of Environment*, **44**, 165–178.

Gastellu-Etchegorry, J. P., Guillevic, P., Zagolski, F., Demarez, V., Trichon, V., Deering, D., and Leroy, M., 1999, Modeling BRF and radiation regime of boreal and tropical forests: I. BRF. *Remote Sensing of Environment*, **68**, 281–316.

Goel, N. S., 1988, Models of vegetation canopy reflectance and their use in estimation of biophysical parameters from reflectance data. *Remote Sensing Reviews*, **4**, 1–212.

Green, R. O., Eastwood, M. L., and Williams, O., 1998, Imaging spectroscopy and the Airborne Visible/Infrared Imaging Spectrometer (AVIRIS). *Remote Sensing of Environment*, **65**, 227–240.

Hapke, B., Dimucci, D., Nelson, R., and Smythe, W., 1996, The cause of the hot spot in vegetation canopies and soils: shadow-hiding versus coherent backscatter. *Remote Sensing of Environment*, **58**, 63–68.

Jacquemoud, S., Baret, F., and Hanocq, J. F., 1992, Modeling spectral and bidirectional soil reflectance. *Remote Sensing of Environment*, **41**, 123–132.

Johnson, L. F., 1994, Multiple view zenith angle observations of reflectance from ponderosa pine stands. *International Journal of Remote Sensing*, **15**, 3859–3865.

Kennedy, R. E., Cohen, W. B., and Takao, G., 1997, Empirical methods to compensate for a view-angle-dependent brightness gradient in AVIRIS imagery. *Remote Sensing of Environment*, **62**, 277–291.

Kleman, J., 1987, Directional reflectance factor distributions for two forest canopies. *Remote Sensing of Environment*, **23**, 83–96.

Li, X., and Strahler, A. H., 1985, Geometric-optical modeling of a coniferous forest canopy. *IEEE Transactions on Geoscience and Remote Sensing*, **23**, 207–221.

Lobell, D. B., Asner, G. P., Law, B. E., and Treuhaft, R. N., 2001, Sub-pixel canopy cover estimation of coniferous forests in Oregon using SWIR imaging spectrometry. *Journal of Geophysical Research*, **106**, 5151–5160.

Meyer, D., Verstraete, M., and Pinty, B., 1995, The effect of surface anisotropy and viewing geometry on the estimation of NDVI from AVHRR. *Remote Sensing Reviews*, **12**, 3–27.

MUSTARD, J. F., STAID, M. L., and FRIPP, W. J., 2001, A semi-analytical approach to the calibration of AVIRIS data to reflectance over water: Application in a temperate estuary. *Remote Sensing of Environment*, **75**, 335–349.

MYNENI, R. B., ROSS, J., and ASRAR, G., 1989, A review on the theory of photon transport in leaf canopies. *Agricultural and Forest Meteorology*, **45**, 1–153.

MYNENI, R. B., NEMANI, R. R., and RUNNING, S. W., 1997, Estimation of global leaf area index and absorbed PAR using radiative transfer models. *IEEE Transactions on Geoscience and Remote Sensing*, **35**, 1380–1395.

PRIVETTE, J. L., FOWLER, C., WICK, G. A., BALDWIN, D., and EMERY, W. J., 1995, Effects of orbital drift on Advanced Very High Resolution Radiometer products: normalized difference vegetation index and sea surface temperature. *Remote Sensing of Environment*, **53**, 164–171.

RANSON, K. J., IRONS, J. R., and WILLIAMS, D. L., 1994, Multispectral bidirectional reflectance of northern forest canopies with the Advanced Solid-state Array Spectroradiometer (ASAS). *Remote Sensing of Environment*, **47**, 276–289.

ROBERTS, D. A., SMITH, M. O., and ADAMS, J. B., 1993, Green vegetation, non-photosynthetic vegetation, and soils in AVIRIS data. *Remote Sensing of Environment*, **44**, 255–269.

RUSSELL, C. A., IRONS, J. R., and DABNEY, P. W., 1997, Bidirectional reflectance of selected BOREAS sites from multiangle airborne data. *Journal of Geophysical Research*, **102**, 29 505–29 516.

SANDMEIER, S. T., and DEERING, D. W., 1999, Structure analysis and classification of boreal forests using airborne hyperspectral BRDF data from ASAS. *Remote Sensing of Environment*, **69**, 281–295.

SMITH, M. O., USTIN, S. L., ADAMS, J. B., and GILLESPIE, A. R., 1990, Vegetation in deserts: I. A regional measure of abundance from multispectral images. *Remote Sensing of Environment*, **31**, 1–26.

SMITH, M. O., ADAMS, J. B., and SABOL, D. E., 1994, Spectral mixture analysis—new strategies for the analysis of multispectral data. In *Imaging Spectrometry—A Tool for Environment Observations*, edited by J. Hill and J. Megier (The Netherlands: Kluwer Academic Publishers), Boston, Massachusetts, pp. 125–144.

VERMOTE, E. F., TANRE, D., DEUZE, J. L., HERMAN, M., and MORCRETTE, J. J., 1997, Second simulation of the satellite signal in the solar spectrum, 6S: an overview. *IEEE Transactions on Geoscience and Remote Sensing*, **35**, 675–686.

WALTER-SHEA, E. A., and NORMAN, J. M., 1991, Leaf optical properties. In *Photon-Vegetation Interactions*, edited by R. B. Myneni and J. Ross (Berlin: Springer-Verlag), pp. 229–251.